

Collective $1/f$ fluctuation by pseudo-Casimir-invariants

Yoshiyuki Y. Yamaguchi*

Department of Applied Mathematics and Physics, Graduate School of Informatics, Kyoto University, Kyoto 606-8501, Japan

Kunihiko Kaneko

Department of Basic Science, University of Tokyo, 3-8-1 Komaba, Meguro-ku, Tokyo 153-8902, Japan

In this study, we propose a universal scenario explaining the $1/f$ fluctuation, including pink noises, in Hamiltonian dynamical systems with many degrees of freedom under long-range interaction. In the thermodynamic limit, the dynamics of such systems can be described by the Vlasov equation, which has an infinite number of Casimir invariants. In a finite system, they become pseudoinvariants, which yield quasistationary states. The dynamics then exhibit slow motion over them, up to the timescale where the pseudo-Casimir-invariants are effective. Such long-time correlation leads to $1/f$ fluctuations of collective variables, as is confirmed by direct numerical simulations. The universality of this collective $1/f$ fluctuation is demonstrated by taking a variety of Hamiltonians and changing the range of interaction and number of particles.

Introduction: The $1/f$ fluctuation is ubiquitous in nature: Certain quantities that fluctuate in time exhibit a power spectrum of the form $1/f^\nu$, where f is the frequency and the exponent ν is typically in the range of $1/2 \lesssim \nu \lesssim 3/2$. The $1/f$ fluctuation, suggesting a long-time correlation, is observed in nature such as vacuum tubes [1], semiconductors [2], spin transport [3], oceans [4, 5], quasars [6], solar wind [7, 8], and proteins [9]. The $1/f$ fluctuation is also observed in model systems of water molecules [10, 11], proteins [12], ferromagnetic bodies [13], and accretion disks [14]. (See, for instance, [15–19] for reviews.)

There have been multiple efforts to understand the mechanism of the $1/f$ fluctuation; however, a coherent explanation remains to be lacking. For instance, the superposition of Lorentzians (see [18, 19], for instance) requires a certain distribution of multiple timescales, but the origin of multiple timescales must be explained. Our strategy here is to restrict our concern to Hamiltonian dynamical systems with many degrees of freedom and search for the possibility of $1/f$ spectra for collective variables, as observed in water molecules [10] and ferromagnetic bodies [13].

In Hamiltonian systems with a few degrees of freedom, the $1/f$ fluctuation has been observed and analyzed by the hierarchical structure of the phase space constructed by the KAM tori and chaotic sea [20–26]. The hierarchical structure is analyzed by perturbation theory in two-degrees-of-freedom systems [27] and is also observed in a symplectic coupled map with 4 particles [28]. Nevertheless, such microscopic hierarchical structures exist only in a certain range for a system with a few degrees of freedom and is thus not generic in systems with many degrees of freedom. Hence, it remains to be elucidated how the $1/f$ fluctuation is generated in the collective motion of many-degree-of-freedom systems.

The aim of this article is to propose a universal scenario for the collective $1/f$ fluctuation in long-range Hamiltonian systems with many degrees of freedom. The target class of systems includes self-gravitating systems, plasmas, geo-

physical flows, trapped ions [29], among others [30–32]. In the thermodynamic limit with an infinite number of particles, the dynamics of such systems can be described by the Vlasov equation, the partial differential equation for the one-particle distribution function [33–35]. This equation is described by the distribution function on the one-particle phase space; therefore, the collective motion is naturally treated through the Vlasov equation.

An important feature of Vlasov dynamics is that they have an infinite number of Casimir invariants. The Casimir-invariants are exact in the thermodynamic limit, but in a system with a finite number of particles, they become pseudoinvariants and fluctuate slowly with time. These pseudo-Casimir-invariants play the role of constraints up to a certain timescale, but they break down in the long timescale, as has also been observed recently in the two-step relaxation of fluctuation amplitude in thermal equilibrium [13]. Such slow motion is owing to the pseudo-Casimir-invariants and one may expect a long time correlation in the dynamics of collective variables, i.e., the collective $1/f$ fluctuation. In the present article, we numerically demonstrate that this is indeed true and propose a general scenario for the collective $1/f$ fluctuation that persists up to the timescale where the constraint by pseudo-Casimir-invariants is effective.

Model: We consider the α -Hamiltonian mean-field (α -HMF) model [36], which is described by the Hamiltonian

$$H_\alpha(q, p) = \sum_{j=0}^{N-1} \frac{p_j^2}{2} + \frac{1}{2N_\alpha} \sum_{j=0}^{N-1} \sum_{k=0}^{N-1} \frac{1 - \cos(q_j - q_k)}{r_{jk}^\alpha}, \quad (1)$$

where $\alpha \geq 0$. This system represents XY spins, each of which is located at a one-dimensional lattice point with a unit lattice spacing. The variable q_j denotes the phase of the j th particle, and p_j is the conjugate momentum. A quantum version of this system can be experimentally realized through trapped ions [29]. Here, the spatial boundary condition is set to be periodic, and accordingly, the distance between the j th and k th particles is defined as $r_{jk} = \min\{|j - k|, N - |j - k|\}$ for $k \neq j$ and $r_{jk} = 1$ for $k = j$. The normalization factor N_α is introduced to ensure the extensivity of energy, as is defined by $N_\alpha = \sum_{k=0}^{N-1} 1/r_{jk}^\alpha$. By taking $\alpha = 0$ with $N_0 = N$, the α -HMF model is reduced to the

* yyama@amp.i.kyoto-u.ac.jp

Hamiltonian mean-field (HMF) model [37, 38]. In the opposite limit, $\alpha \rightarrow \infty$, it can be reduced to the model with the nearest-neighbor couplings with $N_\infty = 3$. Hence, the dependence on the coupling ranging from long to short is investigated by varying the value of α .

Here, we investigate the order parameter defined by $\mathbf{M} = \sum_{j=0}^{N-1} (\cos q_j, \sin q_j) / N$. The α -HMF model shows the second-order phase transition at the specific energy $E_c = 3/4$, which corresponds to the critical temperature $T_c = 1/2$, irrespective of the value of α for $0 \leq \alpha < 1$ [39–41]. The boundary between the long- and short-range is given by $\alpha = 1$, beyond which the mean-field description is not valid. We introduce the scaling $x = j/N$ such that the domain of x is restricted to $x \in [-1/2, 1/2]$ because of the periodic boundary condition.

In the limit $N \rightarrow \infty$, the dynamics of the α -HMF model are described by the Vlasov equation [42]:

$$\frac{\partial F}{\partial t} + \frac{\partial \mathcal{H}[F]}{\partial p} \frac{\partial F}{\partial q} - \frac{\partial \mathcal{H}[F]}{\partial q} \frac{\partial F}{\partial p} = 0, \quad (2)$$

where $F(q, p, x, t)$ is the one-particle distribution function, $\mathcal{H}[F](q, p, x, t)$ is the one-particle Hamiltonian functional defined by

$$\begin{aligned} \mathcal{H}[F] &= \frac{p^2}{2} + \mathcal{V}[F](q, x, t), \\ \mathcal{V}[F] &= \frac{-1}{\kappa_\alpha} \int_{-1/2}^{1/2} dx' \int_{-\pi}^{\pi} dq' \int_{-\infty}^{\infty} dp' \frac{\cos(q - q')}{|x - x'|^\alpha} F(q', p', x', t), \end{aligned} \quad (3)$$

and $\kappa_\alpha = \int_{-1/2}^{1/2} (1/|x|^\alpha) dx$. From the Poisson structure of the Vlasov equation, it is easy to show that a Casimir functional,

$$\mathcal{C}[F](t) = \int_{-1/2}^{1/2} dx \int_{-\pi}^{\pi} dq \int_{-\infty}^{\infty} dp c(F(q, p, x, t)) \quad (4)$$

is a constant of motion for any differentiable function c if $c(F) \rightarrow 0$ in $|p| \rightarrow \infty$ (see the Appendix A) [43]. We stress that the validity of the Vlasov description is guaranteed for $\alpha < 1$, as the integral of κ_α does not converge for $\alpha \geq 1$ [44].

Numerical tests and results: The initial values of $\{(q_k, p_k)\}_{k=0}^{N-1}$ are randomly chosen from the one-particle distribution function in thermal equilibrium:

$$F_{\text{eq}}(q, p; T, M) = A \exp[-(p^2/2 - M \cos q)/T], \quad (5)$$

where A is the normalization factor, and T is temperature. From the rotational symmetry of the system, the direction of the order parameter is set to $\mathbf{M} = (M, 0)$. The magnetization M is determined for a given T by solving the self-consistent equation: $M = \int_{-\pi}^{\pi} dq \int_{-\infty}^{\infty} dp F_{\text{eq}}(q, p; T, M) \cos q$.

The temperature T is introduced to parameterize the set of thermal equilibria. All numerical simulations are performed by integrating the canonical equations of motion associated with the N -body Hamiltonian (1) [45] without thermal noise by using the fourth-order symplectic integrator [46] with the time step $\Delta t = 0.1$.

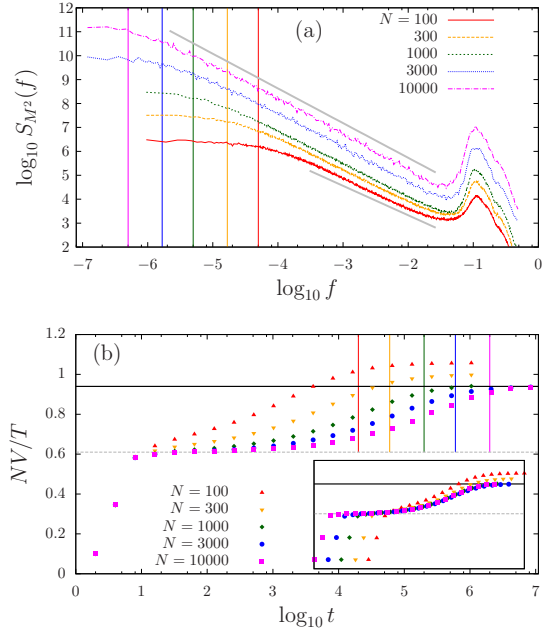


FIG. 1. (color online) N dependence in the HMF model ($\alpha = 0$). $N = 100$ (300, red triangles), 300 (300, orange inverse triangles), 1000 (300, green diamonds), 3000 (50, blue circles), and 10000 (50, magenta squares). The number in parentheses represents the number of sample orbits over which the average is taken. $T = 0.45 (< T_c)$. (a) Power spectra of $M^2(t)$. N increases from bottom to top. For graphical reasons, the vertical scales have been changed suitably. The vertical lines indicate the timescale $1/\tau$ where $\tau = 200N$. The gray line segments guide the eyes for the slopes -1.45 (upper) and -1.23 (lower) obtained by the least-square method in the intervals of segments. (b) Temporal evolution of the scaled variance of magnetization M . The lower gray broken and upper black solid horizontal lines are, respectively, the theoretically predicted plateau level and thermal equilibrium level. N increases from top to bottom. The vertical lines represent $\tau = 200N$. (inset) The horizontal axis is $\log_{10}(t/N)$.

We recall that the Casimir-invariants hold under conditions of (i) thermodynamic limit $N \rightarrow \infty$ and (ii) long-range interaction ($\alpha < 1$). For large but finite N , the Casimir-invariants are no longer invariants; they fluctuate with time, thus becoming pseudoinvariants. To unveil the possible relationship between the pseudo-Casimir-invariants and $1/f$ fluctuation, we first numerically examine the N dependence and α dependence in the low- and high-energy sides of the α -HMF model, respectively.

In the low-energy ordered phase ($T < T_c$), the relationship is examined through the N dependence by fixing the parameter α at $\alpha = 0$ (the HMF model) for simplicity. The power spectra of $M^2(t)$ are presented in Fig. 1(a) for several values of N , which exhibits $1/f$ fluctuations down to a certain frequency τ^{-1} . From the figure, this maximum timescale is estimated as $\tau \sim 200N$, suggesting that the $1/f$ fluctuation persists to small frequencies, in the larger N . The timescale $\tau \propto N$ is consistent with the fact that the collision term of the product of two $O(1/\sqrt{N})$ terms is added to the Vlasov equation (2) for finite N , to break the Casimir

invariants. The power spectra of individual $\cos q_j(t)$ do not exhibit $1/f$ spectra (see the Appendix B), and the observed $1/f$ spectra are caused by collective motion. For a crossover of $1/f$ fluctuation between large and small N , see the Appendix C.

To quantitatively reveal the timescale where the constraint by the pseudo-Casimir-invariants is effective, we also compute the time-dependent variance $V(t)$ defined by

$$V(t) = \sum_{n=0}^{n_0-1} \frac{1}{n_0} \left[\frac{1}{t} \sum_{k=1}^t \|\mathbf{M}(nt+k)\|^2 - \left(\frac{1}{t} \sum_{k=1}^t \|\mathbf{M}(nt+k)\| \right)^2 \right] \quad (6)$$

where $t = 2, 4, 8 \dots$ and n_0 is a sufficiently large number. The variance V is scaled as NV/T , which represents the susceptibility at the thermal equilibrium level, according to the fluctuation-response relation [13]. The temporal evolution of the scaled variance is shown in Fig. 1(b) with indications of the timescale $\tau = 200N$ around which the variance reaches the asymptotic level.

From Fig. 1(b), we can understand that the constraint by the pseudo-Casimir-invariants is effective up to the timescale τ : The small collision term is negligible in the short-time regime and the fluctuation is restricted in the initial Casimir level set, which is an iso-Casimir surface in function space, up to the end of the plateau [47]. The plateau level is theoretically predicted using linear response theory for the Vlasov dynamics [48, 49] under the conservation of the Casimir invariants [50]. With time, the collision term becomes non-negligible, altering the Casimir invari-

ants and moving to another level set. The state is trapped on the new level set (although the next plateau is invisible in the figure because of the logarithmic axis). The change in level sets continues and the cumulative variance (6) thus slowly increases, whereas the suppression by the pseudo-Casimir-invariants remains effective. We underline that the plateau is not perfectly flat, where a perfect plateau suggests that the Casimir invariants are exact as in the limit $N \rightarrow \infty$. The arrival to the asymptotic level at τ suggests that the state has traveled over the possible level sets and the constraint by the pseudo-Casimir-invariants is no longer effective for timescales larger than τ [51].

In the high-energy disordered phase ($T > T_c$), linear response theory predicts that the variance on a Casimir level set agrees with the thermal equilibrium level [48, 52], and, accordingly, no two-step relaxation of $V(t)$ appears (see the Appendix D). In contrast, the disordered phase exists for any value of α . We, therefore, change the strategy and investigate the dependence of the range of interaction α by choosing the initial condition from thermal equilibrium (5) by setting $M = 0$ for $T = 0.6 (> T_c)$. The power spectra of $M^2(t)$ for $T = 0.6$ are presented in Fig. 2 for $N = 32, 1024$, and 8192. As we expected, the $1/f$ spectrum tends to disappear as α increases, i.e., as the interaction range becomes shorter. Moreover, this tendency is enhanced by increasing N and the exponent ν goes to 0 in $\alpha > 1$ as reported in Fig. 2(d). Note that the collective motion is again necessary for observing the $1/f$ spectrum (see the Appendix B). At the low-energy end, a similar figure with Fig. 2 has the same tendency but does not coincide exactly (see the Appendix E).

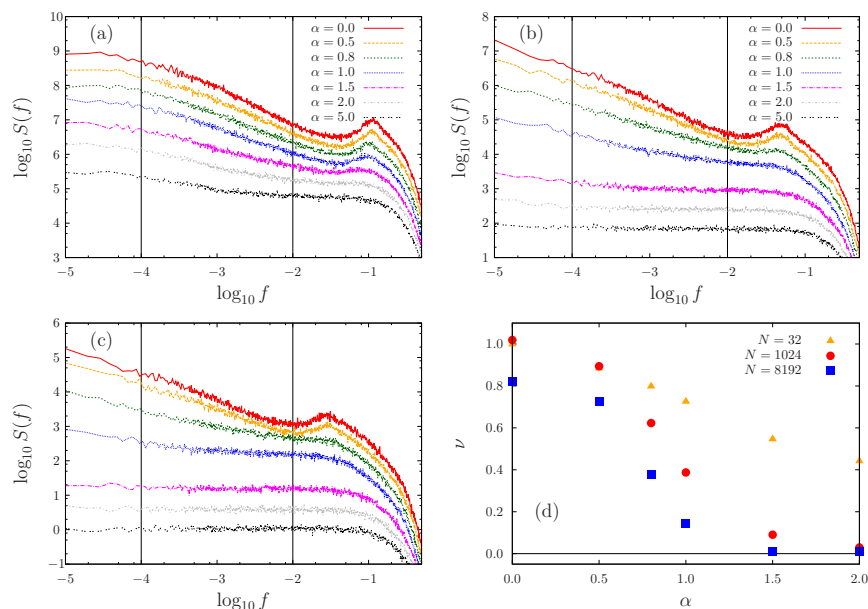


FIG. 2. (color online) Power spectra in the α -HMF model. $T = 0.6$. (a) $N = 32$ (100). (b) $N = 1024$ (100). (c) $N = 8192$ (60). The number in parentheses represents the number of sample orbits. $\alpha = 0, 0.5, 0.8, 1, 1.5, 2$, and 5 from top to bottom. For graphical reasons, the vertical scale has been modified suitably. (d) α dependence of the exponent ν (minus of the slope), which is computed by the least-square method between the two vertical lines of the panels (a)-(c).

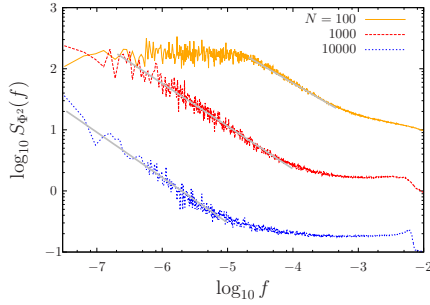


FIG. 3. (color online) Power spectra of $\Phi^2(t)$ in the globally coupled FPUT model. The initial state is in thermal equilibrium with $T = 1$. $N = 100$ (top orange), 1000 (middle red), and 10000 (bottom blue), where the vertical scales of the last two lines have been multiplied by 10 and 100, respectively, for graphical reasons. Each curve is the averages over 20 samples. The time step of simulations is $\Delta t = 0.01$. The initial interval $t \in [0, 10^4]$ has been removed to avoid transience [54]. The gray line segments are obtained from the least-square method in the intervals of segments. The slopes are -0.62 , -0.70 , and -0.74 from top to bottom.

Finally, we investigate whether the existence of phase transition in the α -HMF model is essential to the $1/f$ fluctuation. To this end, we introduce a globally coupled Fermi-Pasta-Ulam-Tsingou (FPUT) system [53]:

$$H_{\text{FPUT}} = \sum_{j=0}^{N-1} \frac{p_j^2}{2} + \frac{1}{2N} \sum_{j=0}^{N-1} \sum_{k=0}^{N-1} \varphi(q_j - q_k), \quad \varphi(q) = \frac{q^2}{2} + \frac{q^4}{4}, \quad (7)$$

which does not exhibit the phase transition. The collective observables that are naïvely expected, such as the variance of q or the potential energy, do not exhibit the $1/f$ fluctuation (see the Appendix F). In contrast, the power spectrum of the collective variable $\Phi^2(t)$ exhibits $1/f$ fluctuation as shown in Fig. 3, where $\Phi = \sum_j (\cos \phi_j, \sin \phi_j) / N$ and ϕ is defined on the (q, p) plane as $(q, p) = (r \cos \phi, r \sin \phi)$ with $r = \sqrt{q^2 + p^2}$. To understand this result, we note that on one Casimir level set, fluctuations should occur on each iso-action curve in the leading order [50], where the action variable is associated with the one-particle Hamiltonian for the thermal equilibrium state. Traveling over level sets gives rise fluctuations over iso-action curves, whereas the angle variable, conjugate with the action variable, captures the long-time correlation (see the Appendix F). The variable ϕ here corresponds to the angle variable [55]. Therefore, Φ is a suitable collective variable to extract the hidden $1/f$ fluctuation arising from the pseudo-Casimir-invariants.

Summary and discussions: In this study, we investigated the origin of the collective $1/f$ fluctuation in many-degree-of-freedom Hamiltonian systems under long-range interaction. Such systems have an infinite number of Casimir invariants in the limit $N \rightarrow \infty$, which, in a finite system, constrains the motion as pseudoinvariants and leads to the slow

motion of collective variables. We then propose a simple but universal scenario: The collective $1/f$ fluctuation appears in the timescale up to which the constraint by the pseudo-Casimir-invariants is effective. This scenario has been successfully verified numerically by investigating the α -HMF model, FPUT model, and the dependence of the power spectra on the number of elements and the interaction range.

As the Casimir-invariants are based on the distribution function and the average of an observable over it gives a collective variable, it is natural that the $1/f$ fluctuation is observed only for collective variables. For local variables such as the position of each particle, such long-term fluctuations are not observed. The collective variable in concern is given by an order parameter, as the average of the angle variable, corresponding to the slow change of the level of pseudo-Casimir-invariants. In the globally coupled FPUT model, the $1/f$ fluctuation may be hidden and is extracted by setting suitable observables with the aid of the proposed scenario.

To confirm the importance of the Casimir invariants (that are based on the Poisson structure of the Vlasov equation), we also examined the Kuramoto model [57], as a non-Hamiltonian and dissipative version of the HMF model, and confirmed that the system does not exhibit $1/f$ fluctuation (see the Appendix G) [58]. The superposition of Lorentzian spectra is also unsuitable to explain the observed $1/f$ fluctuation by considering the timescales determined by the Landau damping modes (see the Appendix H).

It is important to examine the universality of our result. Although we considered the thermal equilibrium states of simple models here, the existence of Casimir invariants does not depend on consideration of reference states or the details of interaction potentials in long-range Hamiltonian systems, and the slow dynamics by pseudo-Casimir-invariants will generally be applied to the so-called quasistationary states [30] for instance. As there exists a variety of examples that can be effectively described by long-range Hamiltonian systems, such as plasmas, free electron laser [30, 59–62], water molecules [63], and trapped ions [29, 64–67], collective $1/f^v$ fluctuation will be experimentally verifiable. In real systems, the Poisson structure providing the Casimir invariants will be disturbed by dissipation and randomness. It will be important to examine the robustness of our scenario under such perturbations. Finally, the theory to predict the exponent v in the $1/f^v$ spectrum must be formulated based on the slow motion of pseudo-Casimir-invariants.

ACKNOWLEDGMENTS

Y.Y.Y. acknowledges the support of JSPS KAKENHI Grant No. 16K05472.

Appendix A: Casimir invariants

Let us consider the Vlasov equation

$$\frac{\partial F}{\partial t} + \frac{\partial \mathcal{H}[F]}{\partial p} \frac{\partial F}{\partial q} - \frac{\partial \mathcal{H}[F]}{\partial q} \frac{\partial F}{\partial p} = 0 \quad (\text{A1})$$

for the one-particle distribution function $F(q, p, x, t)$, where q and p are the conjugate position and momentum, and x represents the spatial position. We prove that a Casimir functional

$$\mathcal{C}[F](t) = \int_{-1/2}^{1/2} dx \int_{-\pi}^{\pi} dq \int_{-\infty}^{\infty} dp c(F(q, p, x, t)) \quad (\text{A2})$$

is a constant of motion if the one-particle Hamiltonian functional $\mathcal{H}[F](q, p, x, t)$ belongs to the C^2 -class with respect to q and p , and if $|c(F(q, p, x, t))|$ rapidly decreases in $|p| \rightarrow \infty$. Differentiating with respect to time t and using the Vlasov equation, we have

$$\begin{aligned} \frac{d\mathcal{C}[F]}{dt} &= \int_{-1/2}^{1/2} dx \int_{-\pi}^{\pi} dq \int_{-\infty}^{\infty} dp c'(F) \left(-\frac{\partial \mathcal{H}[F]}{\partial p} \frac{\partial F}{\partial q} + \frac{\partial \mathcal{H}[F]}{\partial q} \frac{\partial F}{\partial p} \right) \\ &= \int_{-1/2}^{1/2} dx \int_{-\pi}^{\pi} dq \int_{-\infty}^{\infty} dp \left(-\frac{\partial \mathcal{H}[F]}{\partial p} \frac{\partial c(F)}{\partial q} + \frac{\partial \mathcal{H}[F]}{\partial q} \frac{\partial c(F)}{\partial p} \right). \end{aligned} \quad (\text{A3})$$

Performing the integration by parts and noting the rapid decrease in $c(F)$ for $|p| \rightarrow \infty$, we have

$$\frac{d\mathcal{C}[F]}{dt} = \int_{-1/2}^{1/2} dx \int_{-\pi}^{\pi} dq \int_{-\infty}^{\infty} dp c(F) \left(\frac{\partial}{\partial q} \frac{\partial \mathcal{H}[F]}{\partial p} - \frac{\partial}{\partial p} \frac{\partial \mathcal{H}[F]}{\partial q} \right) = 0, \quad (\text{A4})$$

for $\mathcal{H}[F]$ in the C^2 -class. The decreasing speed of $c(F)$ is sufficient to cause the term $c(F)\partial_q \mathcal{H}[F]$ to vanish in the limit $|p| \rightarrow \infty$, and the condition is reduced to $c(F) \rightarrow 0$ for $|p| \rightarrow \infty$ if $\mathcal{H}[F]$ consists of the p -dependent kinetic and q -dependent potential parts.

Appendix B: Power spectra of individual particles

In the α -Hamiltonian mean-field model, no $1/f$ fluctuation occurs in the time series concerning the individual particle. Figures 4 and 5 respectively report flat power spectra for N dependence with $\alpha = 0$ and α dependence with $N = 1024$. We thus conclude that the observed $1/f$ fluctuation comes from collective motion.

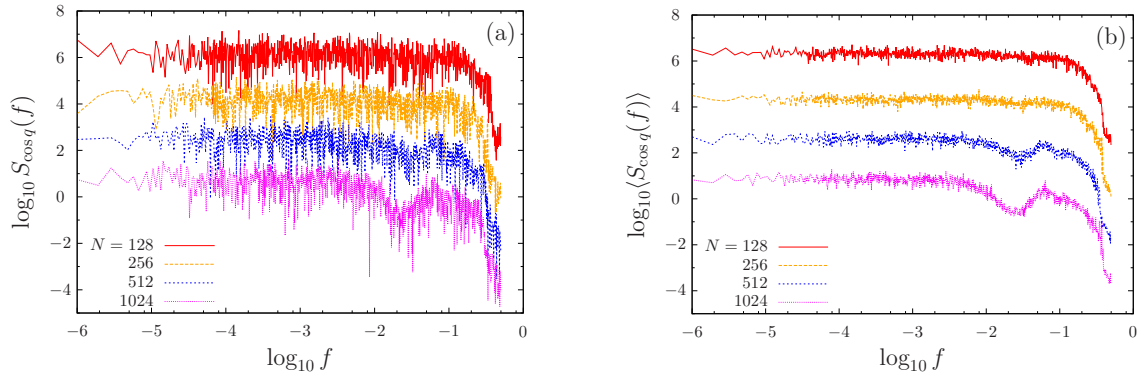


FIG. 4. (color online) (a) Power spectra of $\cos q_0(t)$ and (b) average over N of power spectra of $\cos q_j(t)$ in the α -HMF model. $\alpha = 0$. $T = 0.45$. $N = 128$ (red), 256 (orange), 512 (blue), and 1024 (magenta) from top to bottom, where the horizontal scales have been multiplied by 10^{-2} , 10^{-4} , and 10^{-6} in the last three curves, respectively, for graphical reasons.

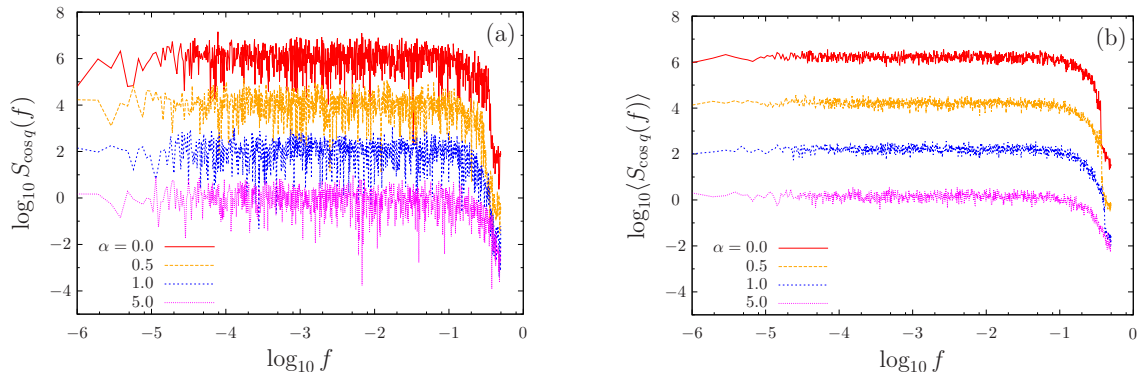


FIG. 5. (color online) (a) Power spectra of $\cos q_0(t)$ and (b) average over N of power spectra of $\cos q_j(t)$ in the α -HMF model. $N = 1024$. $T = 0.6$. $\alpha = 0$ (red), 0.5 (orange), 1 (blue), and 5 (magenta) from top to bottom, where the horizontal scales have been multiplied by 10^{-2} , 10^{-4} , and 10^{-6} in the last three curves, respectively, for graphical reasons.

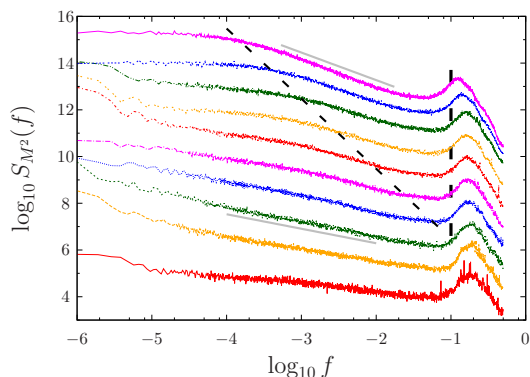


FIG. 6. (color online) Power spectra of $M^2(t)$ in the HMF model ($\alpha = 0$). $T = 0.45 (< T_c)$. $N = 3, 4, \dots, 10, 20$, and 50 from bottom to top. For graphical reasons, the vertical scale has been multiplied by 10^1 for $N = 4$, 10^2 for $N = 5$, etc. Each curve is the average over 100 samples. The gray line segments guide the eyes for the slopes -0.62 (lower) and -1.18 (upper) obtained by the least-square method in the intervals of the segments. The $1/f$ fluctuation due to pseudo-Casimir-invariants is proposed as the enclosed domain by the two black dashed lines.

Appendix C: N dependence in low-energy ordered phase with small N

By further investigating the N dependence of the power spectrum, we note the existence of two distinct types of $1/f$ fluctuation as in Fig. 6. For larger N ($\gtrsim 9$), the collective $1/f$ fluctuation is observed. For smaller N ($3 \lesssim N \lesssim 8$), however, the $1/f$ fluctuation exhibits slopes clearly different from the previous type. One possible explanation of the $1/f$ fluctuation with small N might be the hierarchical structure of phase space [28], whereas we note that 10 particles are sufficiently large to exhibit the collective $1/f$ fluctuation based on the pseudo-Casimir-invariants.

Appendix D: N dependence in high-energy disordered phase

Next, we study the power spectra of the square order parameter and temporal evolution of the variance in the high-energy disordered phase of the Hamiltonian mean-field model ($\alpha = 0$), by setting the temperature to $T = 0.6$ in Fig. 7 and $T = 0.8$ in Fig. 8, where the critical temperature is $T_c = 0.5$. At both temperatures, $1/f$ power spectra are observed, but the slopes -0.70 and -0.64 in the long-time region are quite close to that observed with small N in the low-energy ordered phase. In the high-energy side, the largest Lyapunov exponent tends to vanish as N increases [68–70]. Accordingly, one possible understanding of the small exponent is that the system is nearly integrable and the hierarchical structure appears together with the constraint by the pseudo-Casimir-invariants. The comparison between $T = 0.6$ and $T = 0.8$ supports this hypothesis as the small exponent becomes significant as T increases, where the dynamics are more regular.

At the high-energy side, we define the variance as

$$V(t) = \sum_{n=0}^{n_0-1} \frac{1}{n_0} \left[\frac{1}{t} \sum_{k=1}^t \|\mathbf{M}(nt+k)\|^2 - \left(\frac{1}{t} \sum_{k=1}^t \mathbf{M}(nt+k) \right)^2 \right], \quad (\text{D1})$$

because the order parameter vector \mathbf{M} fluctuates on the two-dimensional plane around $\mathbf{M} = \mathbf{0}$. Both with and without the Casimir constraints, the scaled variance NV/T is theoretically predicted as $NV/T = 2T_c/(T - T_c)$ [13], which is twice the susceptibility. Accordingly, there is no two-step relaxation of variance in Figs. 7(b) and 8(b). The arrival to the thermal equilibrium level, therefore, does not imply the end of effectivity of the pseudo-Casimir-invariants, because the arrival is possible on one Casimir level set.

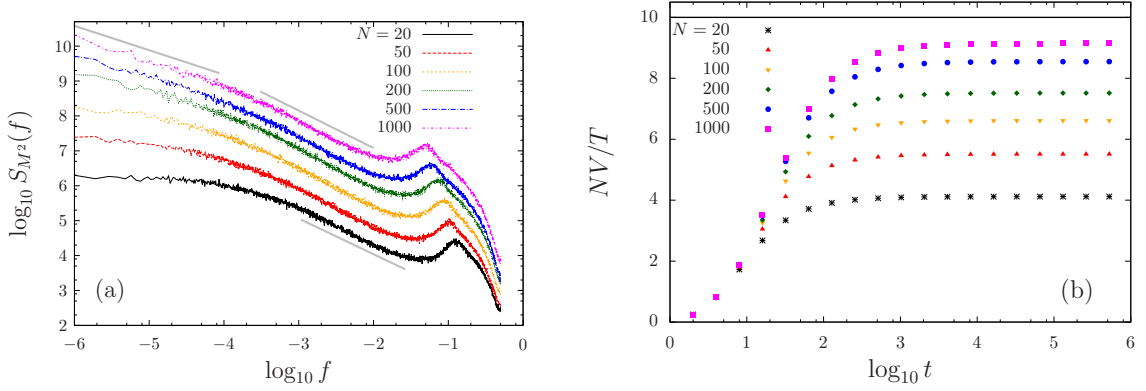


FIG. 7. (color online) N dependence in the HMF model ($\alpha = 0$). $T = 0.60 (> T_c)$. $N = 20$ (black stars), 50 (red triangles), 100 (orange inverse triangles), 200 (green diamonds), 500 (blue circles), and 1000 (magenta squares). (a) Power spectra of $M^2(t)$. N increases from bottom to top. For graphical reasons, the vertical scale has been multiplied by 10^1 for $N = 50$, 10^2 for $N = 100$, etc. The gray line segments guide the eyes for the slopes -0.70 (left upper), -1.07 (right upper), and -1.02 (right lower) obtained by the least-square method in the intervals of segments. (b) Temporal evolution of the scaled variance of magnetization M . N has the same values as those in (a). The black horizontal line represents the thermal equilibrium level, 10. In both panels, each curve is the average over 100 samples.

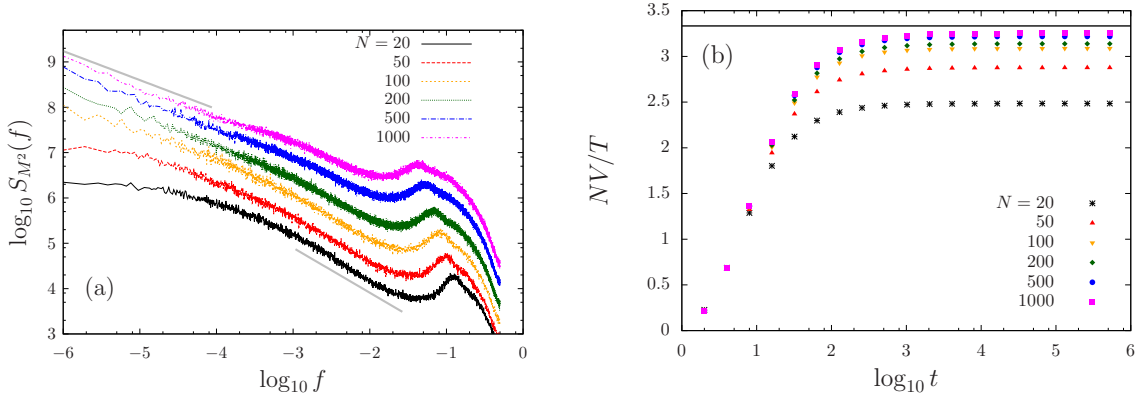


FIG. 8. (color online) Similar to Fig. 7 but with $T = 0.8$. In panel (a), the vertical scales are suitably modified. The gray line segments guide the eyes for the slopes -0.64 (upper left) and -0.99 (lower right) obtained by the least-square method in the intervals of segments. In panel (b), the black horizontal line represents the thermal equilibrium level, $10/3$.

Appendix E: α dependence in low-energy ordered phase

Fixing $T = 0.45 (< T_c)$, we computed power spectra of M^2 by varying the value of α (Fig. 9). Note that, for $\alpha > 1$, the initial condition randomly chosen from the distribution function $A \exp[-(p^2/2 - M \cos q)/T]$ is not guaranteed to be in thermal equilibrium. As in the high-energy disordered phase, the slope of power spectrum goes to zero as α increases, but $\alpha = 1$

seems not the threshold. Instead, the slope goes to zero at α beyond which the ordered phase disappears. We may imagine that, in the low-energy side, wrecks of the Casimir invariants remain for $\alpha \gtrsim 1$. This expectation does not contradict with the fact that the Casimir invariants exist if the interaction is long-range, since validity of the converse is not mentioned. One difficulty studying around $\alpha = 1$ is that N dependence becomes weak as shown in Fig. 10. An in-depth investigation in the middle range of $\alpha \gtrsim 1$ needs to be performed.

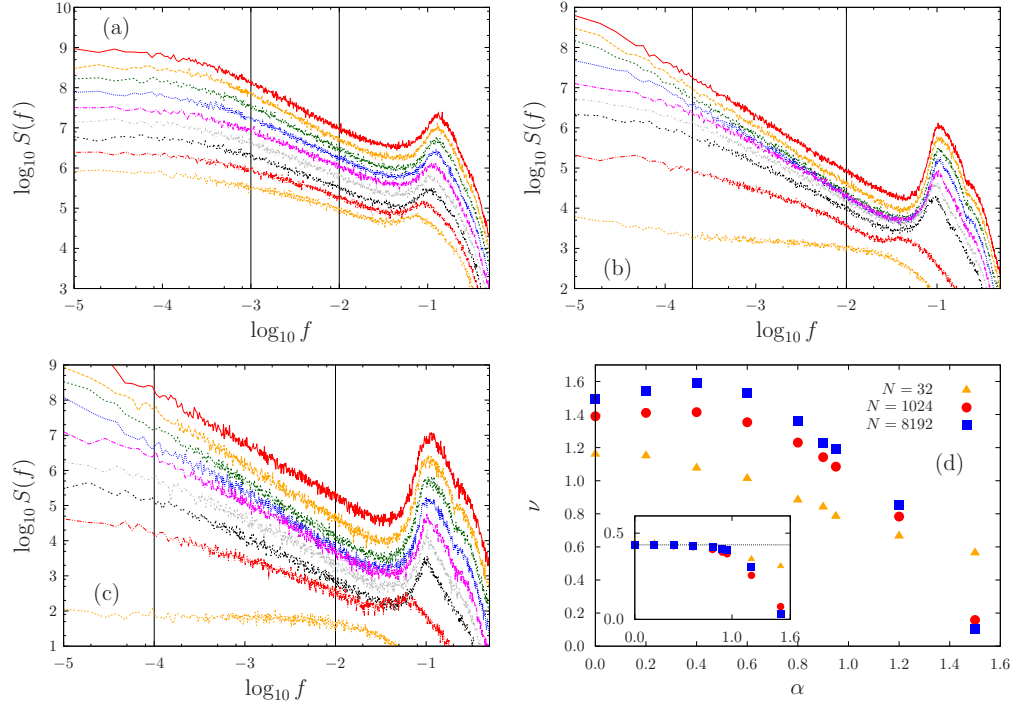


FIG. 9. (color online) Power spectra in the α -HMF model. $T = 0.45$. (a) $N = 32$ (100). (b) $N = 1024$ (100). (c) $N = 8192$ (20). The number in parentheses represents the number of sample orbits. $\alpha = 0$ (red), 0.2 (orange), 0.4 (green), 0.6 (blue), 0.8 (magenta), 0.9 (gray), 0.95 (black), 1.2 (red), and 1.5 (orange) from top to bottom. For graphical reasons, the vertical scale has been modified suitably. (d) α dependence of the exponent ν (minus of the slope), which is computed by the least-square method between the two vertical lines of the panels (a)-(c). $N = 32$ (orange triangles), 1024 (red circles), and 8192 (blue squares). (inset) α dependence of time average of M .

Appendix F: Dependence of observables

In the globally coupled Fermi-Pasta-Ulam-Tsingou system

$$H_{\text{FPUT}} = \sum_{j=0}^{N-1} \frac{p_j^2}{2} + \frac{1}{2N} \sum_{j=0}^{N-1} \sum_{k=0}^{N-1} \varphi(q_j - q_k), \quad \varphi(q) = \frac{q^2}{2} + \frac{q^4}{4}, \quad (\text{F1})$$

we compute the other power spectra of the variance of q ,

$$\Delta = X_2 - X_1^2, \quad X_n = \frac{1}{N} \sum_{j=0}^{N-1} q_j^n, \quad (\text{F2})$$

the potential energy U , and Θ^2 , where the order parameter Θ is defined by

$$\Theta = \frac{1}{N} \sum_{j=0}^{N-1} (\cos \theta_j, \sin \theta_j), \quad (\text{F3})$$

and θ is the angle variable, which is conjugate to the action variable associated with the one-particle Hamiltonian

$$\mathcal{H}_{\text{FPUT}} = \frac{p^2}{2} + \frac{1+3X_2^c}{2} q^2 + \frac{1}{4} q^4. \quad (\text{F4})$$

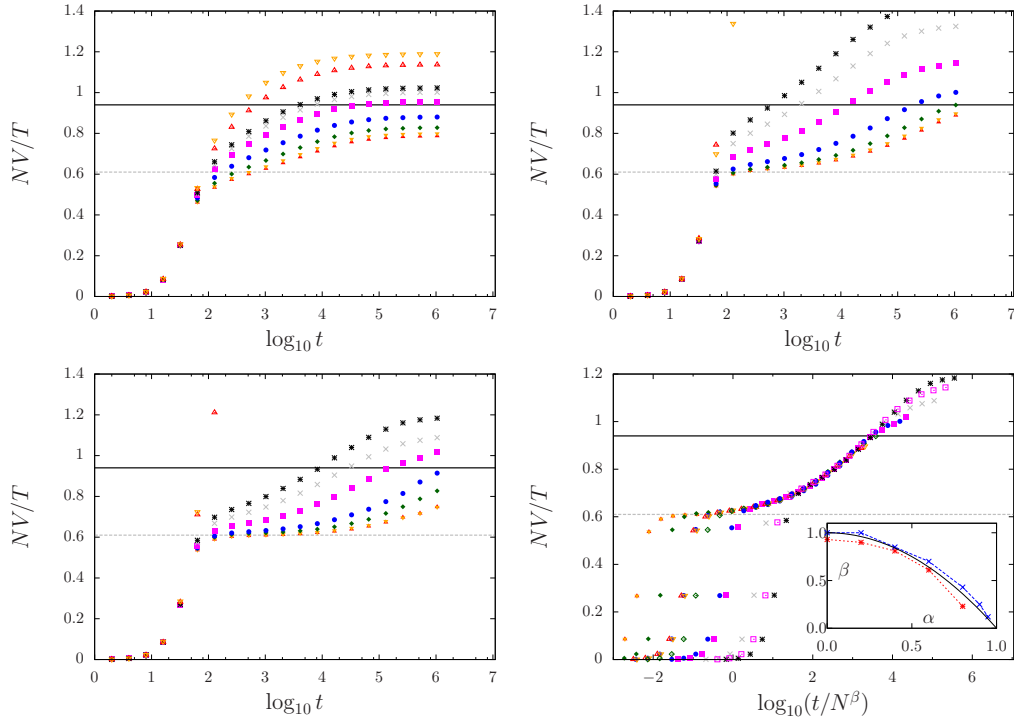


FIG. 10. (color online) Temporal evolution of $V(t)$ in the α -HMF model. $T = 0.45$. (a) $N = 32$ (100). (b) $N = 1024$ (100). (c) $N = 8192$ (20). The number in parentheses represents the number of sample orbits. $\alpha = 0$ (red triangles), 0.2 (orange inverse triangles), 0.4 (green diamonds), 0.6 (blue circles), 0.8 (magenta squares), 0.9 (gray crosses), 0.95 (black stars), 1.2 (red open triangles), and 1.5 (orange open inverse triangles) from bottom to top. The horizontal scales of $\alpha = 1.2$ and 1.5 are out of range for $t > 100$ in (b) and (c). (d) The horizontal axis is scaled as t/N^β . (inset) α dependence of β , which is obtained by fixing $\beta = 1$ for $(N, \alpha) = (8192, 0)$. The lower red and upper blue lines are for $N = 1024$ and $N = 8192$ respectively. The black solid line represents $\beta = 1 - \alpha^2$.

The value of X_2^c is computed to satisfy the self-consistent equation from the canonical thermal equilibrium distribution, which is proportional to $\exp(-\mathcal{H}_{\text{FPUT}}/T)$. For $T = 1$, we have $X_2^c \simeq 0.34252$.

The power spectra are presented in Fig. 11. The variables Δ and U have no $1/f$ fluctuation, but Θ^2 is another suitable observable to find the hidden $1/f$ fluctuation as Φ^2 .

Appendix G: Kuramoto model

The Kuramoto model is expressed as

$$\frac{d\theta_j}{dt} = \omega_j - \frac{K}{N} \sum_{k=1}^N \sin(\theta_j - \theta_k), \quad (\text{G1})$$

where θ_j represents the phase of the j th oscillator, ω_j is the natural frequency depending on the number of oscillators, and $K > 0$ is the coupling constant. The natural frequency ω_j is independently and randomly drawn from a probability distribution function $g(\omega)$. The Kuramoto model describes the synchronization transition from the nonsynchronized state to the partially synchronized state. The extent of synchrony is measured by the order parameter

$$Z = \frac{1}{N} \sum_{k=1}^N e^{i\theta_k}. \quad (\text{G2})$$

If $g(\omega)$ is even and unimodal, then we find the critical coupling constant $K_c = 2/[\pi g(0)]$, where the nonsynchronized state is stable (unstable) for $K < K_c$ ($K > K_c$).

In the limit $N \rightarrow \infty$, the Kuramoto model is described by the equation of continuity

$$\frac{\partial f}{\partial t} + \frac{\partial}{\partial \theta}(vf) = 0, \quad (\text{G3})$$

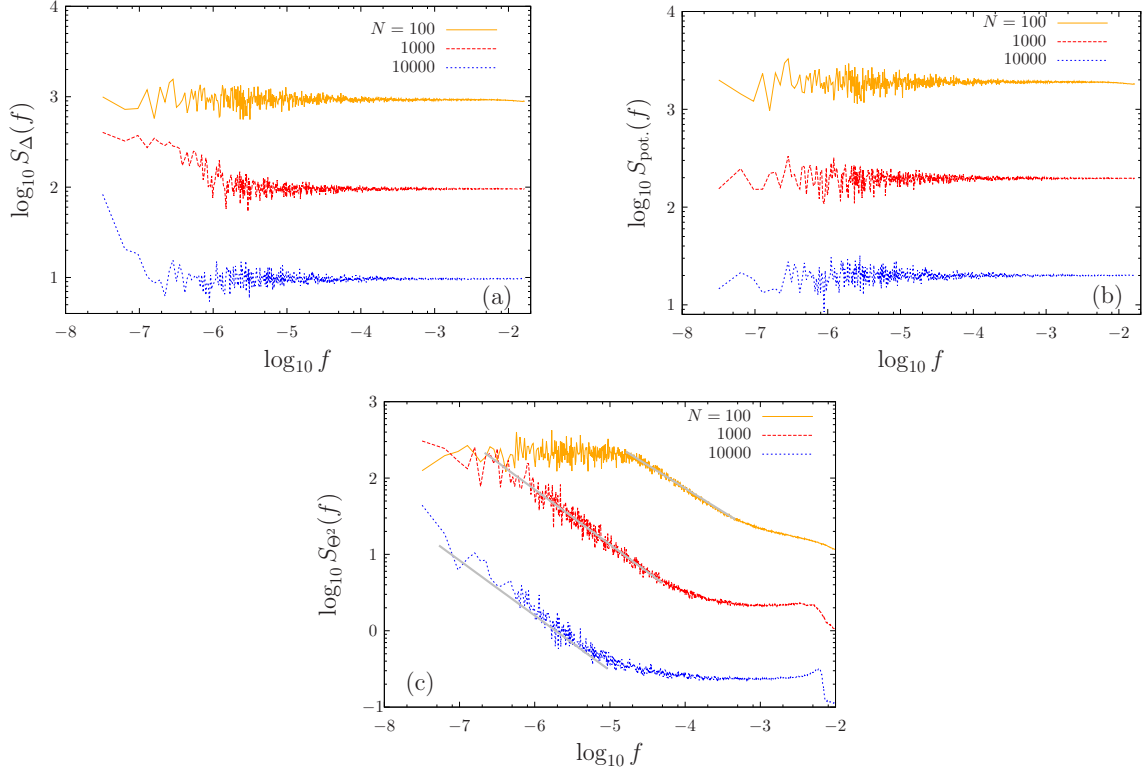


FIG. 11. (color online) Power spectra of (a) Δ , (b) potential energy, and (c) Θ^2 in the globally coupled FPUT model. $T = 1$. $N = 100$ (top orange), 1000 (middle red), and 10000 (bottom blue), where the vertical scales of the last two lines in (c) have been multiplied by 10 and 100, respectively, for graphical reasons. The curves are averages over 20 samples obtained with the time step of $\Delta t = 0.01$. The gray line segments in (c) are obtained by the least square method in the intervals of the segments, and their slopes are -0.61 , -0.72 , and -0.72 for $N = 100$, 1000, and 10000 respectively.

where $f(\theta, \omega, t)$ is the probability distribution function satisfying $\int_0^{2\pi} f(\theta, \omega, t) d\theta = g(\omega)$, and

$$v = \omega - K \int_{-\infty}^{\infty} d\omega' \int_0^{2\pi} d\theta' \sin(\theta - \theta') f(\theta', \omega', t). \quad (\text{G4})$$

The equation of continuity (G3) corresponds to the Vlasov equation (A1). This correspondence becomes clear by rewriting the Vlasov equation in the form

$$\frac{\partial F}{\partial t} + \nabla_{(q,p)} \cdot (\mathbf{X}F) = 0, \quad (\text{G5})$$

where

$$\nabla_{(q,p)} = \left(\frac{\partial}{\partial q}, \frac{\partial}{\partial p} \right) \quad (\text{G6})$$

and \mathbf{X} is the Hamiltonian vector field

$$\mathbf{X} = \left(\frac{\partial \mathcal{H}[f]}{\partial p}, -\frac{\partial \mathcal{H}[f]}{\partial q} \right). \quad (\text{G7})$$

Nevertheless, the equation of continuity has no Poisson structure and no Casimir invariants accordingly. We can not expect $1/f$ fluctuation of collective variables originated from the Casimir mechanism.

To confirm absence of $1/f$ fluctuation in the order parameter, we set $g(\omega)$ as the normal distribution

$$g(\omega) = \frac{1}{\sqrt{2\pi T}} \exp(-\omega^2/2T) \quad (\text{G8})$$

with “temperature” $T = 0.6$, which gives $K_c = 1.236\dots$. We numerically integrate the equation of motion (G1) by using the fourth-order Runge-Kutta method with the time step $\Delta t = 0.1$. The power spectrum of $|Z(t)|^2$ is reported in Fig. 12. The observable is a collective variable, but no $1/f$ fluctuation appears irrespective of values of the coupling constant K .

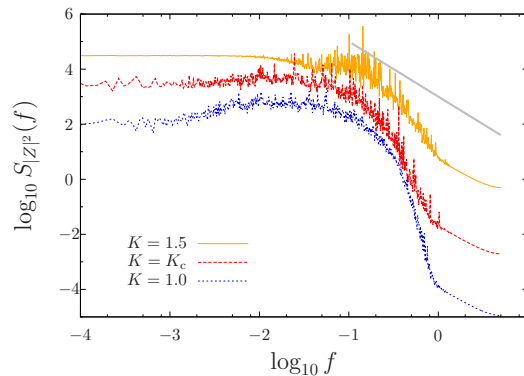


FIG. 12. (color online) Power spectra of $|Z(t)|^2$ in the Kuramoto model. The coupling constant is $K = 1.0$ (blue lower), $K = K_c$ (red middle), and $K = 1.5$ (orange upper). The vertical scale for $K = 1.5$ is multiplied by 10 for graphical reasons. Each curve is the average over 20 samples. The upper gray line segment guides the eyes for the slope -2 .

Appendix H: Superposition of Lorentzian spectra

One traditional explanation of $1/f$ fluctuations is a superposition of Lorentzian spectra originating from the exponentially damping correlation (see [18, 19], for instance). A long-range system has several exponential Landau damping modes in general, but the $1/f$ spectra reported in this article cannot be explained by this superposition: The second slowest damping rate is of $O(1)$ around $T = T_c$ in the α -HMF model, and no accumulation of Landau poles appears in the slow timescale of $f \sim 10^{-3}$.

-
- [1] J. B. Johnson, The schottky effect in low frequency circuits, Phys. Rev. **26**, 71 (1925).
- [2] M. A. Caloyannides, Microcycle spectral estimates of $1/f$ noise in semiconductors, J. Appl. Phys. **45**, 307 (1974).
- [3] S. Omar, M. H. D. Guimarães, A. Kaverzin, B. J. van Wees and I. J. Vera-Marun, Spin relaxation $1/f$ noise in graphene, Phys. Rev. B **95**, 081403(R) (2017).
- [4] C. Wunsch, Bermuda sea level in relation to tides, weather, and baroclinic fluctuations, Rev. Geophys. and Space Phys. **10**, 1 (1972).
- [5] B. A. Taft, B. M. Hickey, C. Wunsch and D. J. Baker, Jr., Equatorial undercurrent and deeper flows in the central Pacific, Deep Sea Research and Oceanographic Abstracts, **21**, 403 (1974).
- [6] M. R. S. Hawkins, Time dilation and quasar variability, ApJ **553**, L97 (2001).
- [7] W. H. Matthaeus and M. L. Goldstein, Low-frequency $1/f$ noise in the interplanetary magnetic field, Phys. Rev. Lett. **57**, 495 (1986).
- [8] W. H. matthaeus, B. Breech, P. Dmitruk, A. Bemporad, G. Polletto, M. Velli and M. Romoli, Density and magnetic field signatures of interplanetary $1/f$ noise, Astrophys. J. **657**, L121 (2007).
- [9] W. Min, G. Luo, B. J. Cherayil, S. C. Kou and X. S. Xie, Observation of a power-law memory kernel for fluctuations within a single protein molecule, Phys. Rev. Lett. **94**, 198302 (2005).
- [10] M. Sasai, I. Ohmine and R. Ramaswamy, Long time fluctuation of liquid water: $1/f$ spectrum of energy fluctuation in hydrogen bond network rearrangement dynamics, J. Chem. Phys. **96**, 3045 (1992).
- [11] E. Yamamoto, T. Akimoto, M. Yasui and K. Yusuoka, Origin of $1/f$ noise in hydration dynamics on lipid membrane surfaces, Sci. Rep. **5**, 8876; DOI:10.1038/srep08876 (2015).
- [12] E. Yamamoto, T. Akimoto, Y. Hirano, M. Yasui and K. Yusuoka, $1/f$ fluctuations of amino acids regulate water transportation in aquaporin 1, Phys. Rev. E **89**, 022718 (2014).
- [13] Y. Y. Yamaguchi, Strange scaling and relaxation of finite-size fluctuation in thermal equilibrium, Phys. Rev. E **94**, 012133 (2016).
- [14] A. Janiuk and R. Misra, Stabilization of radiation pressure dominated accretion disks through viscous fluctuations, A & A **540**, A114 (2012).
- [15] W. H. Press, Flicker noises in astronomy and elsewhere, Comments on Astrophysics **7**, 103 (1978).
- [16] P. Dutta and P. M. Horn, Low-frequency fluctuations in solids: $1/f$ noise, Rev. Mod. Phys. **53**, 497 (1981).
- [17] M. B. Weissman, $1/f$ noise and other slow, nonexponential kinetics in condensed matter, Rev. Mod. Phys. **60**, 537 (1988).
- [18] E. Milotti, $1/f$ noise: a pedagogical review, arXiv:physics/0204033.
- [19] L. M. Ward and P. E. Greenwood, $1/f$ noise, Scholarpedia **2**(12), 1537 (2007).
- [20] Y. Aizawa, Symbolic dynamics approach to the two-dimensional chaos in area-preserving maps: A fractal geometrical model, Prog. Theor. Phys. **71**, 1419–1421 (1984).
- [21] J. D. Meiss and E. Ott, Markov-Tree model of intrinsic transport in Hamiltonian systems, Phys. Rev. Lett. **55**, 2741–2744 (1985).
- [22] J. D. Meiss, Class renormalization: Islands around islands, Phys. Rev. A **34**, 2375–2383 (1986).
- [23] J. D. Meiss and E. Ott, Markov tree model of transport in area-preserving maps, Physica D **20**, 387–402 (1986).
- [24] T. Geisel, A. Zacherl and G. Radons, Generic $1/f$ noise in chaotic Hamiltonian dynamics, Phys. Rev. Lett. **59**, 2503–2506 (1987).

- [25] Y. Aizawa, Y. Kikuchi, T. Harayama, K. Yamamoto, M. Ota and K. Tanaka, Stagnant motions in Hamiltonian systems, *Prog. Theor. Phys. Suppl.* **98**, 36–82 (1989).
- [26] Y. Y. Yamaguchi and T. Konishi, A geometrical model for stagnant motion in Hamiltonian systems with many degrees of freedom, *Prog. Theor. Phys.* **99**, 139–144 (1998).
- [27] A. J. Lichtenberg and M. A. Leiberman, *Regular and Chaotic Dynamics, Second Edition* (Springer-Verlag, New York, 1992).
- [28] T. Konishi and K. Kaneko, Clustered motion in symplectic coupled map systems, *J. Phys. A: Math. Gen.* **25**, 6283 (1992).
- [29] P. Richerme, Z.-X. Gong, A. Lee, C. Senko, J. Smith, M. Foss-Feig, S. Michalakis, A. V. Gorshkov and C. Monroe, Non-local propagation of correlations in quantum systems with long-range interactions, *Nature* **511**, 198–201 (2014).
- [30] A. Campa, T. Dauxois and S. Ruffo, Statistical mechanics and dynamics of solvable models with long-range interactions, *Phys. Rep.* **480**, 57 (2009).
- [31] Y. Levin, R. Pakter, F. B. Rizzato, T. N. Teles and F. P. C. Benetti, Nonequilibrium statistical mechanics of systems with long-range interactions, *Phys. Rep.* **535**, 1 (2014).
- [32] A. Campa, T. Dauxois, D. Fanelli and S. Ruffo, *Physics of Long-Range Interacting Systems* (Oxford University Press, Oxford, 2014).
- [33] W. Braun and K. Hepp, The Vlasov dynamics and its fluctuations in the $1/N$ limit of interacting classical particles, *Commun. Math. Phys.* **56**, 101 (1977).
- [34] R. L. Dobrushin, Vlasov equations, *Funct. Anal. Appl.* **13**, 115 (1979).
- [35] H. Spohn, *Large Scale Dynamics of Interacting Particles* (Springer-Verlag, Heidelberg, 1991).
- [36] C. Anteneodo and C. Tsallis, Breakdown of exponential sensitivity to initial conditions: Role of the range of interactions, *Phys. Rev. Lett.* **80**, 5313 (1998).
- [37] S. Inagaki and T. Konishi, Dynamical stability of a simple model similar to self-gravitating systems, *Publ. Astron. Soc. Japan* **45**, 733 (1993).
- [38] M. Antoni and S. Ruffo, Clustering and relaxation in Hamiltonian long-range dynamics, *Phys. Rev. E* **52**, 2361 (1995).
- [39] F. Tamarit and C. Anteneodo, Rotators with long-range interactions: Connection with the mean-field approximation, *Phys. Rev. Lett.* **84**, 208 (2000).
- [40] A. Campa, A. Giansanti and D. Moroni, Canonical solution of a system of long-range interacting rotators on a lattice, *Phys. Rev. E* **62**, 303 (2000).
- [41] T. Mori, Analysis of the exactness of mean-field theory in long-range interacting systems, *Phys. Rev. E* **82**, 060103(R) (2010).
- [42] R. Bachelard, T. Dauxois, G. De Ninno, S. Ruffo and F. Staniscia, Vlasov equation for long-range interactions on a lattice, *Phys. Rev. E* **83**, 061132 (2011).
- [43] In our study, F rapidly goes to zero in $|p| \rightarrow \infty$ and $c(F) = F^n$ ($n = 1, 2, \dots$) make Casimir invariants, for instance.
- [44] We note that the divergence of κ_α can be avoided by introducing, for instance, long-range-like coupling constants in the interval $x \in [-\epsilon, \epsilon]$ with small $\epsilon > 0$. However, the scaling $x = j/N$ says that the particle at $x = 0$ interacts with an infinite number of particles in a long-range manner, and the short-range nature disappears accordingly. The case $\alpha = 1$ is included in the long-range coupling, but we do not discuss this boundary case.
- [45] For $N = 2^n$, $n \in \mathbb{N}$, the interaction coefficient matrix, $R = (1/(N_\alpha r_{jk}^\alpha))$, is diagonalized by the fast Fourier transform (FFT) matrix. By using this diagonalization and the FFT algorithm, we can reduce the numerical cost of the α -HMF model from $O(N^2)$ to $O(N \log N)$. This trick helps to perform long-time evolution.
- [46] H. Yoshida, Recent progress in the theory and application of symplectic integrators, *Celestial Mechanics and Dynamical Astronomy* **56**, 27 (1993).
- [47] The initial increase in $V(t)$ for $t < 10$ comes from the definition (6), which gives $V(1) = 0$.
- [48] S. Ogawa and Y. Y. Yamaguchi, Linear response theory in the Vlasov equation for homogeneous and for inhomogeneous quasistationary states, *Phys. Rev. E* **85**, 061115 (2012).
- [49] S. Ogawa and Y. Y. Yamaguchi, Landau-like theory for universality of critical exponents in quasistationary states of isolated mean-field systems, *Phys. Rev. E* **91**, 062108 (2015).
- [50] Y. Y. Yamaguchi and S. Ogawa, Conditions for predicting quasistationary states by rearrangement formula, *Phys. Rev. E* **92**, 042131 (2015).
- [51] The constraint by the pseudo-Casimir-invariants remains, even after the variance reaches the asymptotic level. Thus, a similar evolution of $V(t)$ is obtained against the shift of the initial time [13].
- [52] A. Patelli, S. Gupta, C. Nardini and S. Ruffo, Linear response theory for long-range interacting systems in quasistationary states, *Phys. Rev. E* **85**, 021133 (2012).
- [53] T. Dauxois, Fermi, Pasta, Ulam, and a mysterious lady, *Physics Today* **61**, 55 (2008).
- [54] No transience has been observed in the HMF model [13], so this procedure was skipped in the HMF model.
- [55] The variable ϕ does not completely agree with the angle variable which should be obtained with the action variable by the canonical transform of (q, p) [56], but ϕ approximately represents the angular motion.
- [56] H. Goldstein, C. Poole and J. Safko, *Classical Mechanics, 3rd ed.* (Addison-Wesley, 2001).
- [57] Y. Kuramoto, Self-entrainment of a population of coupled non-linear oscillators, in H. Araki (Ed.) *International Symposium on Mathematical Problems in Theoretical Physics* (Springer-Verlag, Berlin Heidelberg, 1975) pp.420–422.
- [58] D. García-Gudiño, E. Landa, J. Mendoza-Temis, A. Albarado-Ibañez, J. C. Toledo-Roy, I. O. Morales and A. Frank, Enhancement of early warning properties in the Kuramoto model and in an atrial fibrillation model due to an External perturbation of the system, *PLoS One* **12**, e0181953 (2017).
- [59] W. B. Colson, Theory of a free electron laser, *Phys. Lett. A* **59**, 187 (1976).
- [60] R. Bonifacio, C. Pellegrini and L. M. Narducci, Collective instabilities and high-gain regime in a free electron laser, *Optical Communications* **50**, 373 (1984).
- [61] G. M. Zaslavskii, V. F. Shabanov, K. S. Aleksandrov, I. P. Aleksandrova, A model for a phase transition due to nonlinear resonance of lattice vibrations, *Sov. Phys. JETP* **45**, 315 (1977).
- [62] J. Barré, T. Dauxois, G. De Ninno, D. Fanelli and S. Ruffo, Statistical theory of high-gain free-electron laser saturation, *Phys. Rev. E* **69**, 045501(R) (2004).
- [63] W. L. Jorgensen, Transferable intermolecular potential functions for water, alcohols, and ethers. Application to liquid water, *J. Am. Chem. Soc.* **103**, 335 (1981).
- [64] D. Porras and J. I. Cirac, Effective Quantum Spin Systems with Trapped Ions, *Phys. Rev. Lett.* **92**, 207901 (2004).
- [65] K. Kim, M.-S. Chang, R. Islam, S. Korenblit, L.-M. Duan and C. Monroe, Entanglement and Tunable Spin-Spin Couplings between Trapped Ions Using Multiple Transverse Modes, *Phys. Rev. Lett.* **103**, 120502 (2009).

- [66] J. W. Britton, B. C. Sawyer, A. C. Keith, C.-C. J. Wang, J. K. Freericks, H. Uys, M. J. Biercuk, J. J. John, and J. Bollinger, Engineered Two-Dimensional Ising Interactions in a Trapped-Ion Quantum Simulator with Hundreds of Spins, *Nature (London)* **484**, 489 (2012).
- [67] R. Islam, C. Senko, W. C. Campbell, S. Korenblit, J. Smith, A. Lee, E. E. Edwards, C.-C. J. Wang, J. K. Freericks and C. Monroe, Emergence and Frustration of Magnetism with Variable-Range Interactions in a Quantum Simulator, *Science* **340**, 583-587 (2013).
- [68] Y. Y. Yamaguchi, Slow relaxation at critical point of second order phase transition in a highly chaotic Hamiltonian system, *Prog. Theor. Phys.* **95**, 717 (1996).
- [69] V. Latora, A. Rapisarda, S. Ruffo, Lyapunov instability and finite size effects in a system with long-range forces, *Phys. Rev. Lett.* **80**, 692 (1998).
- [70] M.-C. Firpo, Analytic estimation of the Lyapunov exponent in a mean-field model undergoing a phase transition, *Phys. Rev. E* **57**, 6599 (1998).